Phase diagram and thermal expansion measurements on the system $URu_{2-x}Fe_xSi_2$

Sheng Ran[a,b], Christian T. Wolowiec[a,b], Inho Jeon[b,c], Naveen Pouse[a,b], Noravee Kanchanavatee[a,b,1], Benjamin D. White[a,b,2], Kevin Huang[b,c,3], Dinesh Martien[d], Tyler DaPron[d], David Snow[d], Mark Williamsen[d], Stefano Spagna[d], Peter S. Riseborough[e], and M. Brian Maple[a,b,c,4]

[a]Department of Physics, University of California, San Diego, La Jolla, CA 92093; [b]Center for Advanced Nanoscience, University of California, San Diego, La Jolla, CA 92093; [c]Materials Science and Engineering Program, University of California, San Diego, La Jolla, CA 92093; [d]Quantum Design, Inc., San Diego, CA 92121; and [e]Physics Department, Temple University, Philadelphia, PA

Contributed by M. Brian Maple, October 6, 2016 (sent for review July 23, 2016); reviewed by Zachary Fisk and Marcelo Jaime

Thermal expansion, electrical resistivity, magnetization, and specific heat measurements were performed on $URu_{2-x}Fe_xSi_2$ single crystals for various values of Fe concentration x in both the hidden-order (HO) and large-moment antiferromagnetic (LMAFM) regions of the phase diagram. Our results show that the paramagnetic (PM) to HO and LMAFM phase transitions are manifested differently in the thermal expansion coefficient. The uniaxial pressure derivatives of the HO/LMAFM transition temperature T_0 change dramatically when crossing from the HO to the LMAFM phase. The energy gap also changes consistently when crossing the phase boundary. In addition, for Fe concentrations at $x_c \approx 0.1$, we observe two features in the thermal expansion upon cooling, one that appears to be associated with the transition from the PM to the HO phase and another one at lower temperature that may be due to the transition from the HO to the LMAFM phase.

hidden order | URu_2Si_2 | thermal expansion

The search for the order parameter of the hidden-order (HO) phase in URu_2Si_2 has attracted an enormous amount of attention for the past three decades (1–4). The small antiferromagnetic moment of only $\sim$0.03 μ_B/U found in the HO phase is too small to account for the entropy of $\sim 0.2R\ln(2)$ derived from the second-order mean-field Bardeen–Copper–Schrieffer (BCS)-like specific heat anomaly associated with the HO transition that occurs below $T_0 = 17.5$ K (2, 5). A first-order transition from the HO phase to a large-moment antiferromagnetic (LMAFM) phase occurs under pressure at a critical pressure P_c that lies in the range 0.5–1.5 GPa (6–9). Many studies suggest that the HO and LMAFM phases are intimately related and that a comprehensive investigation of both phases will be useful in unraveling the nature of the order parameter of the HO phase (10). Although the order parameters are presumably different in the HO and LMAFM phases, the two phases exhibit almost indistinguishable transport and thermodynamic properties. This behavior has been referred to as "adiabatic continuity" (11).

We have recently demonstrated that tuning URu_2Si_2 by substitution of Fe for Ru affords an opportunity to study both the HO and LMAFM phases and the HO-LMAFM phase transition at atmospheric pressure (12–14). Specifically, the substitution of the smaller Fe ions for Ru ions in URu_2Si_2 appears to act as a chemical pressure such that the temperature vs. Fe concentration ($T - x$) phase diagram for the $URu_{2-x}Fe_xSi_2$ system resembles the temperature vs. applied pressure ($T - P$) phase diagram for URu_2Si_2. In a previous study, neutron diffraction measurements on single-crystal samples of $URu_{2-x}Fe_xSi_2$ for various values of x (13) revealed that the magnetic moment increases abruptly to a maximum value at $x = 0.1$, above which it then decreases slowly with x, supporting the interpretation that tuning by Fe substitution acts as a chemical pressure.

On the other hand, the phase boundary between the HO and LMAFM phases has not been definitively determined for the $URu_{2-x}Fe_xSi_2$ system. Extensive effort has been expended to map out the precise phase boundary between the HO and LMAFM phases in URu_2Si_2 under pressure, which is not vertical on the $T - P$ phase diagram (8, 9, 15–19). The critical pressure at which the HO–LMAFM transition occurs is about 1.5 GPa at T_0, whereas it drops to about 0.8 GPa at the base temperature (9). Therefore, at intermediate values of pressure, e.g., 1 GPa, URu_2Si_2 goes through two successive phase transitions upon cooling: a second-order transition from the paramagnetic (PM) into the HO phase and then a first-order transition from the HO into the LMAFM phase. The HO–LMAFM transition upon cooling has not been observed in either polycrystalline or single-crystal samples of $URu_{2-x}Fe_xSi_2$. It is possible that in the polycrystalline samples, both the PM–HO and HO–LMAFM transitions are broadened, especially in the vicinity of the HO–LMAFM phase boundary, so that the transition from the HO phase into the LMAFM phase with decreasing temperature is not readily discernible. The identity of the order parameter of the HO phase in the compound URu_2Si_2 remains a long-standing mystery. The HO phase is intimately related to

Significance

The identity of the order parameter of the hidden-order (HO) phase in the heavy fermion compound URu_2Si_2 remains a long-standing mystery. The HO phase is intimately related to the large-moment antiferromagnetic (LMAFM) phase that is induced under pressure. Although these two phases presumably have distinct order parameters, their transport and thermodynamic properties are nearly indistinguishable. The measurements reported herein reveal that the HO and LMAFM phase transitions are manifested differently in the uniaxial thermal expansion coefficients and uniaxial pressure derivatives of the transition temperature. These results suggest that an itinerant effective model should include band states of different orbital and magnetic characters, if it is to describe the differing responses of the competing ordered phases to uniaxial pressure.

Author contributions: S.R. and M.B.M. designed research; S.R., C.T.W., I.J., N.P., N.K., B.D.W., K.H., D.M., T.D., and D.S. performed research; D.M., T.D., D.S., M.W., and S.S. contributed new reagents/analytic tools; S.R. and P.S.R. analyzed data; and S.R., C.T.W., and M.B.M. wrote the paper.

Reviewers: Z.F., University of California, Irvine; M.J., Los Alamos National Laboratory.

The authors declare no conflict of interest.

[1]Present address: Department of Physics, Chulalongkorn University, Pathumwan 10330, Thailand.

[2]Present address: Department of Physics, Central Washington University, Ellensburg, WA 98926.

[3]Present address: State Key Laboratory of Surface Physics, Department of Physics, Fudan University, Shanghai 200433, China.

[4]To whom correspondence should be addressed. Email: mbmaple@ucsd.edu.

the LMAFM phase that is induced under pressure. Although these two phases have distinct order parameters, their transport and thermodynamic properties are nearly indistinguishable. The measurements reported herein reveal that the HO and LMAFM phase transitions are manifested differently in the uniaxial thermal expansion coefficients and uniaxial pressure derivatives of the transition temperature. These results suggest that an itinerant effective model should include band states of different orbital and magnetic characters, if it is to describe the differing responses of the competing ordered phases to uniaxial pressure.

In the experiments reported herein, we performed thermal expansion, electrical resistivity, magnetization, and specific heat measurements on $URu_{2-x}Fe_xSi_2$ single crystals for various values of x throughout the PM, HO, and LMAFM regions of the $T - x$ phase diagram. Our thermal expansion measurements reveal differences in the features associated with the PM to HO and LMAFM phase transitions that appear in the thermal expansion coefficient, reflecting differences in the coupling of the two phases to the lattice. The uniaxial pressure derivative of the transition temperature, based on an analysis using thermal expansion and specific heat data, changes dramatically when crossing from the HO to the LMAFM phase. In addition, for Fe concentrations near the boundary between the HO and LMAFM phases at $x_c \approx 0.1$, two features in the thermal expansion are found upon cooling, one that appears to be associated with the transition from the PM to the HO phase and another at lower temperature that may be due to the transition from the HO to the LMAFM phase. These two features have not been observed in other measurements such as specific heat or neutron scattering.

Results

Shown in Fig. 1*A* are electrical resistivity $\rho(T)$ data, normalized to values at 250 K, for various $URu_{2-x}Fe_xSi_2$ compounds. The $\rho(T)$ curves are offset vertically for clarity. For this study, we focus on the interrelation of the HO and LMAFM phases. Therefore, we did not perform low-temperature measurements to study superconductivity. The transition from the PM into the HO phase in the parent compound is manifested as an anomaly at around 17 K. The transition temperature T_0 is defined as the minimum in $d\rho/dT$. Upon Fe substitution, the signature of the phase transition is preserved, whereas T_0 changes systematically. After an initial suppression to 16.2 K at $x = 0.08$, T_0 increases up to 34 K at $x = 0.7$. Similar results are obtained from magnetization $M(T)$ data, as shown in Fig. 1*B*. The corresponding feature for the phase transition in $M(T)$ is the slope change. The transition temperature can be extracted from the quantity $d(MT)/dT$

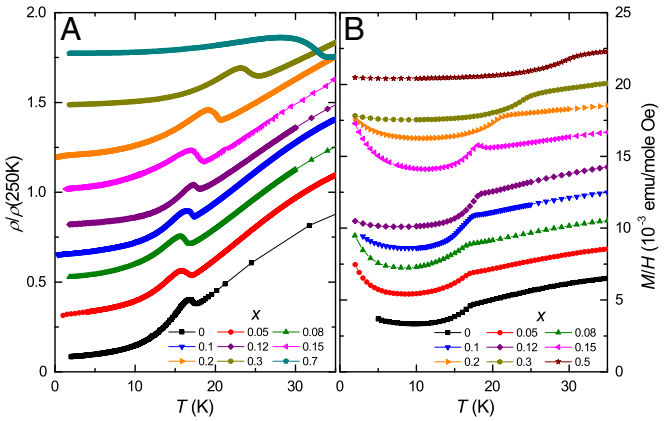

Fig. 1. (*A*) Electrical resistivity ρ and (*B*) magnetization M vs. T for $URu_{2-x}Fe_xSi_2$ single crystals with various values of x between 0 and 0.7. The electrical resistivity ρ is normalized to values at 250 K.

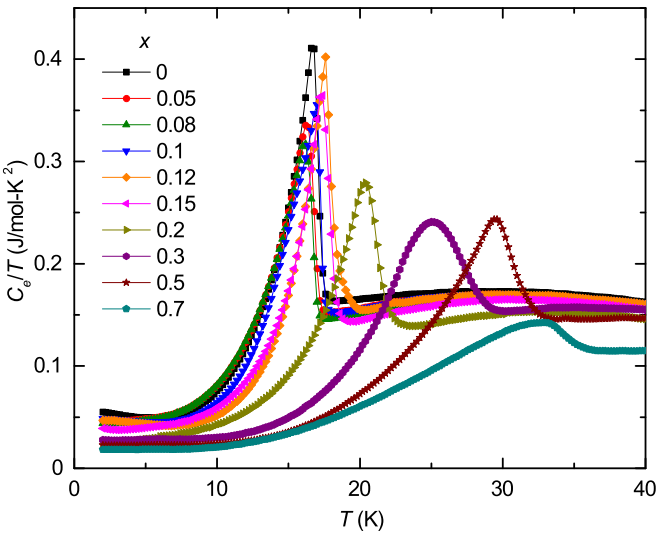

Fig. 2. Electronic specific heat divided by temperature, C_e/T, vs. temperature T for $URu_{2-x}Fe_xSi_2$ single crystals with various values of x between 0 and 0.7.

(see Fig. 4), which is expected to yield a feature that is similar in shape to that observed in the specific heat (20). Although the signature of the phase transition in both $\rho(T)$ and $M(T)$ seems to remain unchanged across the entire Fe concentration range measured in this study, the neutron diffraction experiments indicate that the ground state of $URu_{2-x}Fe_xSi_2$ changes from the HO to the LMAFM phase, with a phase boundary close to $x_c = 0.1$ at low temperatures of the order of 1 K (13).

Displayed in Fig. 2 is the electronic contribution to the specific heat, $C_e(T)$, divided by temperature T, vs. T, determined by subtracting the phonon contribution to the specific heat $C_{ph}(T)$ from the measured specific heat $C(T)$, as discussed in our previous work (12). The electronic specific heat $C_e(T)$ exhibits a well-defined BCS-like anomaly at T_0 upon transition from the PM into the HO and LMAFM phases.

The size of the jump at T_0 remains nearly constant as x increases to 0.15, after which it decreases substantially for the sample with $x = 0.2$. This result indicates that the transition from the HO to the LMAFM phase along the HO–LMAFM phase boundary occurs at a value of x_c between 0.15 and 0.2 and that for x smaller than x_c, the system consists primarily of the HO phase with only a small amount of the LMAFM phase. The size of the jump at the transition decreases above $x = 0.15$ and broadens considerably at $x = 0.7$. In our previous work on polycrystalline samples, a broad shoulder above T_0 was observed and attributed to disorder (12). There is no sign of the broad shoulder in the C_e vs. T data for the single crystals.

Presented in Fig. 3 *A* and *B* are the linear thermal expansion coefficients in the *ab* plane, α_{ab}, and along the *c* axis, α_c, vs. temperature T for $URu_{2-x}Fe_xSi_2$ single crystals with various values of x between 0 and 0.7. The linear thermal expansion coefficient is strongly anisotropic, with α_{ab} positive and α_c negative. At the HO–LMAFM phase transition, an anomaly is observed in both α_{ab} and α_c. However, the signature of the anomaly is markedly different for the PM to HO and LMAFM transitions, showing that the HO and LMAFM phases are clearly distinct from one another. For $x < 0.05$, where the compounds exhibit a PM–HO phase transition, the size of the jump at T_0 is relatively weak, whereas, for larger x, where the LMAFM phase is the ground state, the size of the jump at T_0 is more than three times larger. Similar differences in the size of the jumps in α_{ab} and α_c for the PM–HO and PM–LMAFM transitions have

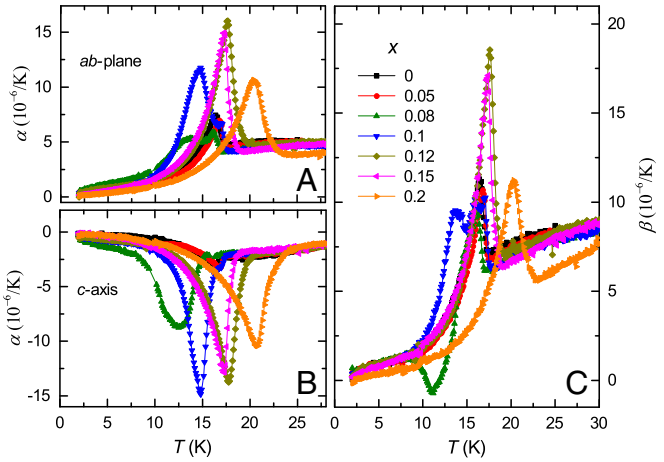

Fig. 3. Linear thermal expansion coefficients (*A*) in the *ab* plane (α_{ab}) and (*B*) along the *c* axis (α_c) vs. temperature *T* for $URu_{2-x}Fe_xSi_2$ single crystals with various values of *x* between 0 and 0.2. (*C*) The calculated volume thermal expansion coefficient, β, vs. *T* derived from the α_{ab} and α_c vs. *T* data in *A* and *B*, respectively.

been reported for URu_2Si_2 under pressure (21). One of the basic features of URu_2Si_2 is the significant amount of coupling of the HO phase to the lattice (22). However, the net volume change is even larger for the PM–LMAFM phase transition, as shown in Fig. 3*C*, indicating that the LMAFM phase is even more strongly coupled to the lattice than the HO phase.

It is noteworthy that for $x = 0.08$ and 0.1, there are two separate anomalies observed in both directions of $\alpha(T)$, as well as in $\beta(T)$, indicating two distinct phase transitions. In both the $x = 0.08$ and 0.1 samples, the sizes of the features at higher temperature are comparable to one another and also consistent with the features observed at the second-order PM-HO phase transition in those samples with lower Fe concentrations. This result suggests that the jump in the thermal expansion coefficient at higher temperature in the $x = 0.08$ and 0.1 samples is likely to be a manifestation of the second-order PM–HO phase transition. On the other hand, the size of the features in $\alpha(T)$ at lower temperatures in the $x = 0.08$ and 0.1 samples is probably due to the phase transition from the HO phase to the LMAFM phase. However, the size of the jump at lower temperature in the $x = 0.08$ sample is smaller than the size of the jump at lower temperature in the $x = 0.10$ sample (Fig. 4). It is likely that only a portion of the sample undergoes a phase transition from the HO phase to the LMAFM phase, and the difference in the size of the jumps in α at lower temperature is a consequence of the difference in volume fraction of samples undergoing this phase transition.

Hence, for the $x = 0.08$ and 0.1 samples, there appears to be a second-order PM–HO phase transition followed at lower temperature by a first-order HO–LMAFM phase transition. It is worth noting that in previous studies of the parent compound URu_2Si_2 under applied pressure, successive phase transitions from the PM phase to the HO phase and then from the HO phase to the LMAFM phase were also observed in electrical resistivity, specific heat, and thermal expansion measurements (18, 21, 23). However, in both the electrical resistivity and specific heat measurements, the anomalies observed at lower temperature corresponding to a first-order transition from the HO phase to the LMAFM phase are much weaker compared with those of the second-order phase transitions from the PM to the HO/LMAFM phases (18). The absence of well-defined features in the electrical resistivity and specific heat associated with the HO–LMAFM phase transition in the parent compound under pressure is consistent with transport and thermodynamic measurements of the Fe-substituted samples of URu_2Si_2 reported in this study, where the first-order HO–LMAFM phase transition is not clearly reflected in electrical resistivity, magnetization, or specific heat measurements (as shown in Fig. 4).

Discussion

Based on the electrical resistivity, magnetization, specific heat, and thermal expansion data, we were able to establish the $T-x$ phase diagram for the $URu_{2-x}Fe_xSi_2$ single crystals shown in Fig. 5. The LMAFM phase becomes stable at $x \approx 0.1$ where the PM–LMAFM phase boundary intersects the PM–HO phase boundary. For further increases in Fe concentration, the PM–LMAFM phase boundary increases to 34 K at $x = 0.7$. This overall behavior is reminiscent of what was previously observed in the dependence of the HO–LMAFM phase boundary on pressure for single crystals of the parent compound URu_2Si_2, indicating that the interpretation of Fe substitution as a chemical pressure (12) also applies to the single crystals.

It is clear that for the intermediate levels of Fe concentration, $x = 0.8$ and 0.1, there are two distinct phase transitions as observed in the thermal expansion measurements. The transitions occurring at lower temperatures help identify the phase boundary between the HO and LMAFM phases. This HO–LMAFM phase boundary can be extended to zero temperature somewhere between $x = 0.05$ and 0.08. It is now believed that the HO and LMAFM phases exhibit different symmetry with distinct order parameters. According to Landau theory, there should be a first-order phase transition between the two phases with different symmetry. However, no obvious hysteresis has been observed in thermal expansion measurements, which indicates that the HO–LMAFM transition is weakly first order.

To further investigate the two distinct phase transitions detected at intermediate Fe concentrations, thermal expansion measurements were performed in magnetic fields up to 9 T on a $URu_{2-x}Fe_xSi_2$ single crystal with $x = 0.1$. The magnetic field was applied along the *c* axis, which is the easy axis, and the thermal expansion was measured in the same direction. The results are shown in Fig. 6. Both transitions are systematically suppressed to lower temperatures by the magnetic field. However, the rate of suppression is clearly different; the higher temperature transition

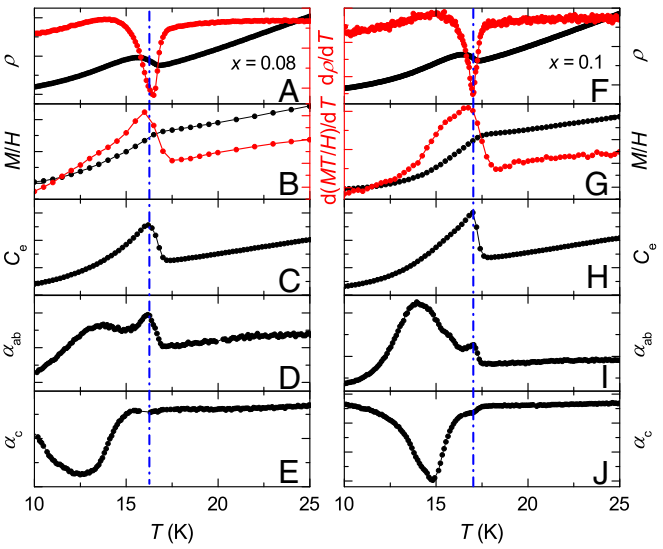

Fig. 4. Normalized electrical resistivity ρ/ρ (250 K), magnetization M/H, electronic specific heat C_e, thermal expansion coefficient in the *ab*-plane α_{ab} and along the *c*-axis α_c vs. *T* for a $URu_{2-x}Fe_xSi_2$ single crystal with $x = 0.08$ (*A*–*E*) and $x = 0.1$ (*F*–*J*). Derivatives of ρ/ρ (250 K) and MT/H with respect to *T* vs. *T* are shown in red.

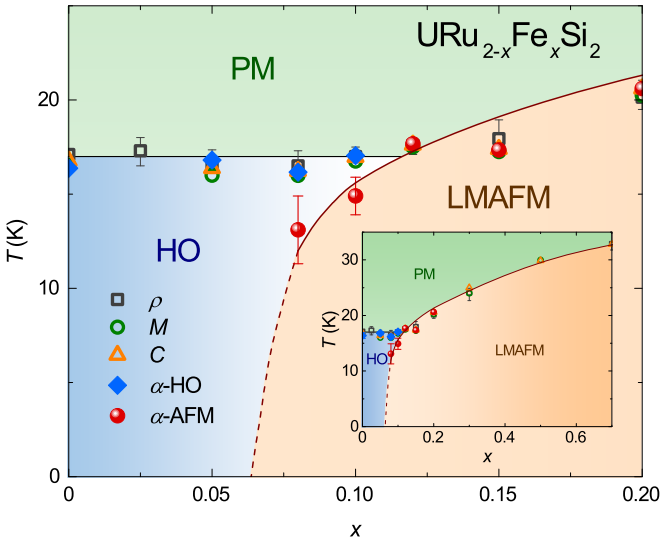

Fig. 5. Temperature T vs. Fe concentration x-phase diagram for the $URu_{2-x}Fe_xSi_2$ system. The phase diagram is based on measurements of electrical resistivity, magnetization, specific heat, and thermal expansion coefficient as a function of temperature on single-crystal specimens.

is reduced only slightly, whereas the lower temperature transition is suppressed more rapidly at a rate of 7.5 K/T. The behavior of the two transition temperatures as a function of magnetic field is shown in Fig. 6, *Inset*. These results, together with resistivity data in high magnetic field (24), are consistent with our hypothesis that the transition at higher temperature is the PM–HO phase transition, whereas the one at lower temperature is the HO–LMAFM phase transition.

At the onset of the HO phase, as well as the LMAFM phase, there is a reconstruction of the Fermi surface, as revealed by transport and thermodynamic measurements (1, 2, 25). For the parent compound, an energy gap associated with the HO phase, originally attributed to a charge or spin density wave (2), opens over about 40% of the Fermi surface. To determine how the energy gap evolves upon Fe substitution, we have evaluated the size of the gap by performing fits of relevant theoretical models to features observed in measurements of the electrical resistivity, specific heat, and thermal expansion coefficient that characterize the HO and LMAFM phases.

Below T_0, the electrical resistivity $\rho(T)$ consists of contributions from the residual resistivity ρ_0, Fermi liquid electron–electron scattering, and electron–magnon scattering due to spin excitations with an energy gap Δ. Because the magnons have antiferromagnetic character, the following expression for $\rho(T)$ is appropriate (26):

$$\rho(T) = \rho_0 + AT^2 + B\Delta^2\sqrt{\frac{T}{\Delta}} \times\left[1+\frac{2}{3}\left(\frac{T}{\Delta}\right)+\frac{2}{15}\left(\frac{T}{\Delta}\right)^2\right]\exp\left(-\frac{\Delta}{T}\right). \quad [1]$$

The specific heat $C_e(T)$ displays a well-defined, BCS-like anomaly upon transition into the HO and LMAFM phases at T_0. Below the transition, the $C_e(T)$ data can be described by the expression:

$$C_e(T) = A\exp\left(-\frac{\Delta}{T}\right)+\gamma T, \quad [2]$$

where γ is the electronic specific-heat coefficient (2). The volume thermal expansion coefficient, $\beta(T)$, exhibits a BCS-like anomaly upon transition into the HO and LMAFM phases as well. Therefore, the $\beta(T)$ data can be described by a similar expression:

$$\beta(T) = C\exp\left(-\frac{\Delta}{T}\right)+AT. \quad [3]$$

The gap values extracted from the three types of measurements are shown in Fig. 7, together with fits of Eqs. **1**–**3** to the data. Although the magnitudes of the gaps are different for the three types of measurements, the gaps follow a consistent trend. The gap values for the HO phase are relatively small, ∼100 K from thermal expansion, ∼80 K from specific heat, and ∼60 K from electrical resistivity. When crossing from the HO to the LMAFM phase (x = 0.1 and 0.12), the gap value is suddenly enhanced by ∼20 K. This is consistent with what has been seen for URu_2Si_2 under pressure (7, 8), as well as recent results for Fe-substituted URu_2Si_2 under pressure (27).

For second-order phase transitions, the uniaxial pressure derivatives of the transition temperature, dT_0/dP, can be estimated using the Ehrenfest relation (28),

$$\frac{dT_0}{dP_i} = V_m T_0 \frac{\Delta\alpha_i}{\Delta C_p}, \quad [4]$$

where V_m is the molar volume that can be calculated from lattice parameters, $\Delta\alpha_i$ is the change in the linear (i = a, c) or volume (α_v = β) thermal expansion coefficient at the phase transition, and ΔC_p is the change in the specific heat at the phase transition. The inferred uniaxial pressure derivatives are shown in Fig. 8. Note that for x = 0.08 and 0.1, both the PM–HO and PM–LMAFM phase transitions were detected in thermal expansion measurements, whereas only the PM–HO phase transition was detected in specific heat measurements. Therefore, for x = 0.08 and 0.1, Eq. **4** allows for an estimate of dT_0/dP only for the HO phase. dT_0/dP has different signs for the two crystallographic orientations. Uniaxial pressure applied along the a or b axes should produce an increase in T_0, whereas uniaxial pressure applied along the c axis should result in a decrease in T_0. Another striking feature is that dT_0/dP changes dramatically when crossing the HO–LMAFM phase boundary. For the HO phase, dT_0/dP_i is relatively small, 0.6 K/GPa for in-plane uniaxial pressure and −0.2 K/GPa for c-axis uniaxial pressure, and does not vary much with Fe concentration. On the other hand, for the LMAFM phase, the magnitude of

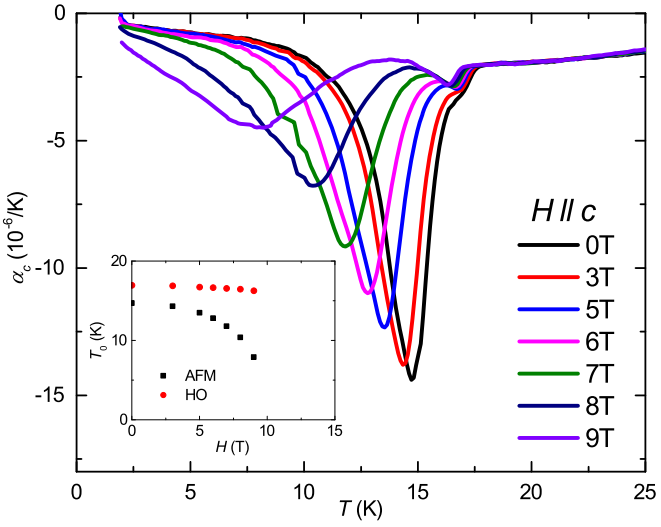

Fig. 6. Thermal expansion coefficient along the c axis vs. temperature T for a $URu_{2-x}Fe_xSi_2$ single crystal with x = 0.1 in magnetic fields up to 9 T. The magnetic field was applied along the c axis. *Inset* shows the magnetic field dependence of the two transition temperatures.

$\mathrm{d}T_0/\mathrm{d}P_i$ is significantly enhanced to above 2 K/GPa for both orientations.

For hydrostatic pressure, $\mathrm{d}T_0/\mathrm{d}P$ can be calculated using the expression

$$\frac{\mathrm{d}T_0}{\mathrm{d}P_V} = 2\frac{\mathrm{d}T}{\mathrm{d}P_a} + \frac{\mathrm{d}T}{\mathrm{d}P_c}, \qquad [5]$$

which also shows a dramatic change upon crossing the HO–LMAFM phase boundary. $\mathrm{d}T_0/\mathrm{d}P$ for the hydrostatic pressure, estimated using the Ehrenfest relation, can be qualitatively compared with recent results of direct measurements of the electrical resistivity of $URu_{2-x}Fe_xSi_2$ under pressure (27), which are also shown in Fig. 8. The two sets of data match quite well over the entire range of Fe concentration, except for $x = 0.1$. At this concentration, the measured value of $\mathrm{d}T_0/\mathrm{d}P$ seems to be closer to that of the LMAFM phase. However, as noted above, the value of $\mathrm{d}T_0/\mathrm{d}P$ for $x = 0.1$ is estimated for the HO phase only and, therefore, does not fully account for the measured value of $\mathrm{d}T_0/\mathrm{d}P$.

The dramatic change in $\mathrm{d}T_0/\mathrm{d}P$ upon crossing from the HO to the LMAFM phase needs to be addressed theoretically, and a possible approach is outlined below. The chemical substitution and pressure dependencies of the PM–HO and HO–LMAFM transition temperatures appear to be related to the lattice parameters c and a. Many experiments (11, 29–32) indicate that both phases evolve from an itinerant paramagnetic phase through Fermi-surface nesting with the same commensurate wave vector $\underline{Q} = (0, 0, 1)$. In particular, the experiments show that as the temperature is lowered below the respective transition temperatures, the nesting gives way to gapping and reconstruction of the Fermi surface. Furthermore, density functional calculations (33) also indicate that $5f$ electronic states at the Fermi energy with $j = \frac{5}{2}$ and $j_z = \pm\frac{5}{2}$ are connected by the same $\underline{Q}$ to $j = \frac{5}{2}$ states with $j_z = \pm\frac{3}{2}$ character. The average number of $5f$ electrons in the lower-energy spin-orbit level $j = \frac{5}{2}$ is approximately given by $n_{f,\frac{5}{2}} \approx 2.35$, whereas the number of $5f$ electrons in the higher-energy $j = \frac{7}{2}$ spin-orbit level is about $n_{f,\frac{7}{2}} \approx 0.65$, consistent with a spin-orbit coupling strength of $\zeta(3) \approx 0.21$ eV and a $5f$ bandwidth of $2 \sim 3$ eV (33). Using the abovementioned

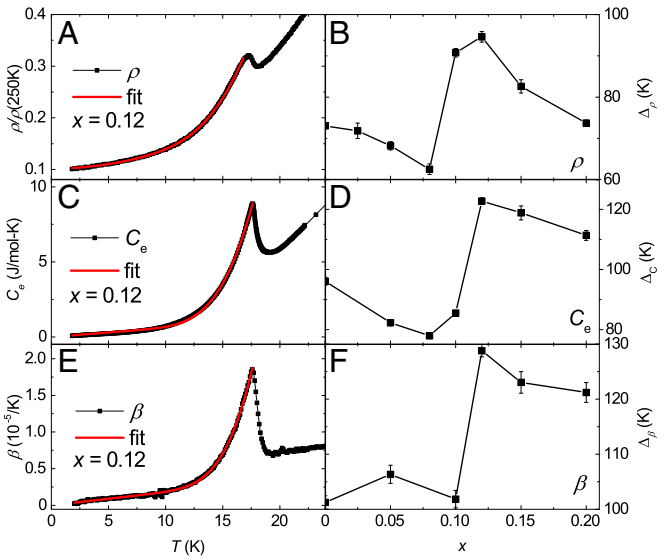

Fig. 7. Representative fits of the expressions given in the text to the (*A*) electrical resistivity $\rho(T)$, (*C*) electronic specific heat $C_e(T)$, and (*E*) volume thermal expansion coefficient $\beta(T)$ data and values of the energy gaps Δ_ρ, Δ_C, and Δ_β, extracted from the fits (*B*, *D*, and *F*).

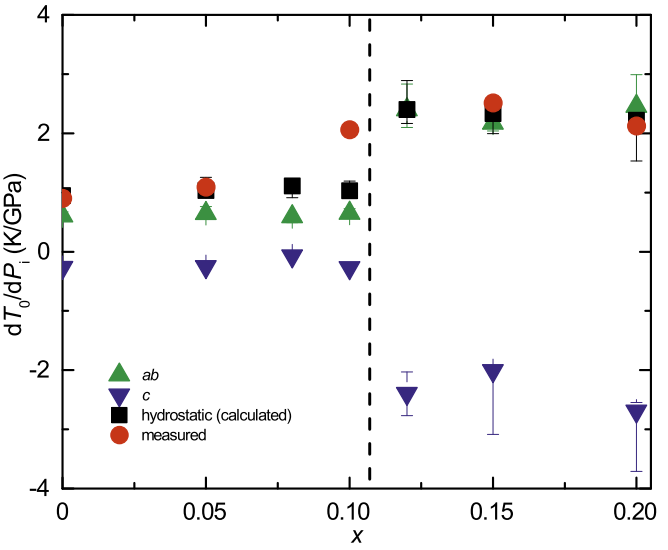

Fig. 8. Uniaxial pressure derivatives of the transition temperature, T_0, estimated using the Ehrenfest relation, as well as from direct measurement.

character of the $5f$ states involved in the Fermi-surface gapping, by projecting onto the Hilbert space spanned by $j_z = \pm\frac{5}{2}$ and $j_z = \pm\frac{3}{2}$, we obtain an effective itinerant model for the low-energy excitations. Within this itinerant effective model, we can investigate a number of possible competing orderings involving $\underline{Q}$, two of which describe AFM phases and a third that may be a candidate for the HO phase. Calculations based on the model described above, along the lines of ref. 34, are currently in progress.

Concluding Remarks

We have performed thermal expansion, electrical resistivity, magnetization, and specific heat measurements on $URu_{2-x}Fe_xSi_2$ single crystals for various values of x between 0 and 0.7, in both the HO and LMAFM regions of the phase diagram. Our results show that the PM–HO and PM–LMAFM phase transitions are expressed differently in the thermal expansion coefficient. The uniaxial pressure derivatives of the HO/LMAFM transition temperature T_0 change dramatically when crossing from the HO to the LMAFM phase. The energy gap also changes consistently when crossing the phase boundary. In addition, by means of thermal expansion measurements, we observed a possible phase transition from the HO into the LMAFM phase for intermediate levels of Fe substitution, which has not been observed in other types of measurements.

Materials and Methods

Single crystals of Fe-substituted URu_2Si_2 were grown by the Czochralski method in a tetra-arc furnace. Electrical resistivity measurements were performed using a home-built probe in a liquid ^{4}He Dewar by means of a standard four-wire technique at 16 Hz, using a Linear Research LR700 ac-resistance bridge. Magnetization measurements were made in a magnetic field of 0.1 T, using a Quantum Design magnetic property measurement system (MPMS). Specific heat measurements were performed in a Quantum Design Dynacool physical property measurement system (DC-PPMS-9), using a heat-pulse technique. Thermal expansion measurements were made in a Quantum Design DC-PPMS-9 with a dilatometer measurement option (model P680). For thermal expansion measurements, the samples were polished into a rectangular shape, approximately 2×3 mm in the *ab* plane and 1 mm along the *c* axis.

ACKNOWLEDGMENTS. Single-crystal growth and characterization at University of California, San Diego (UCSD) was supported by the US Department of Energy, Office of Basic Energy Sciences, Division of Materials Sciences and Engineering, under Grant DEFG02-04-ER46105. Low-temperature measurements at UCSD were sponsored by the National Science Foundation

under Grant DMR 1206553. High-pressure research at UCSD was supported by the National Nuclear Security Administration under the Stewardship Science Academic Alliance Program through the Department of Energy under Grant DE-NA0002909. P.S.R. acknowledges support from the US Department of Energy, Office of Basic Energy Sciences, through Award DE FG02-01ER45872.

1. Palstra TTM, et al. (1985) Superconducting and magnetic transitions in the heavy-fermion system uranium ruthenium silicide (URu_2Si_2). *Phys Rev Lett* 55:2727–2730.
2. Maple MB, et al. (1986) Partially gapped Fermi surface in the heavy-electron superconductor uranium ruthenium silicide (URu_2Si_2). *Phys Rev Lett* 56:185–188.
3. Schlabitz W, et al. (1986) Superconductivity and magnetic order in a strongly interacting Fermi-system: Uranium ruthenium silicide (URu_2Si_2). *Z Phys B Condens Matter* 62:171–177.
4. Mydosh JA, Oppeneer PM (2011) Colloquium: Hidden order, superconductivity, and magnetism: The unsolved case of URu_2Si_2. *Rev Mod Phys* 83:1301–1322.
5. Broholm C, et al. (1987) Magnetic excitations and ordering in the heavy-electron superconductor uranium ruthenium silicide (URu_2Si_2). *Phys Rev Lett* 58:1467–1470.
6. Amitsuka H, et al. (1999) Effect of pressure on tiny antiferromagnetic moment in the heavy-electron compound URu_2Si_2. *Phys Rev Lett* 83:5114–5117.
7. Jeffries JR, Butch NP, Yukich BT, Maple MB (2007) Competing ordered phases in URu_2Si_2: Hydrostatic pressure and rhenium substitution. *Phys Rev Lett* 99: 217207.
8. Motoyama G, Yokoyama N, Sumiyama A, Oda Y (2008) Electrical resistivity and thermal expansion measurements of URu_2Si_2 under pressure. *J Phys Soc Jpn* 77: 123710.
9. Butch NP, et al. (2010) Antiferromagnetic critical pressure in URu_2Si_2 under hydrostatic conditions. *Phys Rev B* 82:060408(R).
10. Bourdarot F, et al. (2010) Precise study of the resonance at Q_0 = (1,0,0) in URu_2Si_2. *J Phys Soc Jpn* 79:064719.
11. Jo YJ, et al. (2007) Field-induced Fermi surface reconstruction and adiabatic continuity between antiferromagnetism and the hidden-order state in URu_2Si_2. *Phys Rev Lett* 98:166404.
12. Kanchanavatee N, et al. (2011) Twofold enhancement of the hidden-order/large-moment antiferromagnetic phase boundary in the $URu_{2-x}Fe_xSi_2$ system. *Phys Rev B* 84:245122.
13. Das P, et al. (2015) Chemical pressure tuning of URu_2Si_2 via isoelectronic substitution of Ru with Fe. *Phys Rev B* 91:085122.
14. Hall JS, et al. (2015) Electrodynamics of the antiferromagnetic phase in URu_2Si_2. *Phys Rev B* 92:195111.
15. Bourdarot F, et al. (2005) Hidden order in URu_2Si_2. *Phys B Condens Matter* 359–361:986–993.
16. Amitsuka H, et al. (2007) Pressure-temperature phase diagram of the heavy-electron superconductor. *J Magn Magn Mater* 310:214–220.
17. Amitsuka H, et al. (2008) Dependence of pressure-induced phase transitions on pressure-transmitting media in the heavy-electron superconductor URu_2Si_2. *Phys B Condens Matter* 403:925–927.
18. Hassinger E, et al. (2008) Temperature-pressure phase diagram of URu_2Si_2 from resistivity measurements and ac calorimetry: Hidden order and Fermi-surface nesting. *Phys Rev B* 77:115117.
19. Niklowitz PG, et al. (2010) Parasitic small-moment antiferromagnetism and nonlinear coupling of hidden order and antiferromagnetism in URu_2Si_2 observed by Larmor diffraction. *Phys Rev Lett* 104:106406.
20. Fisher ME (1962) Relation between the specific heat and susceptibility of an antiferromagnet. *Philos Mag* 7:1731–1743.
21. Motoyama G, Nishioka T, Sato NK (2003) Phase transition between hidden and antiferromagnetic order in URu_2Si_2. *Phys Rev Lett* 90:166402.
22. de Visser A, et al. (1986) Thermal expansion and specific heat of monocrystalline URu_2Si_2. *Phys Rev B* 34:8168–8171.
23. Kambe S, et al. (2013) Thermal expansion under uniaxial pressure in URu_2Si_2. *Phys Rev B* 87:115123.
24. Aoki D, et al. (2009) Field reentrance of the hidden order state of URu_2Si_2 under pressure. *J Phys Soc Jpn* 78:053701.
25. Schoenes J, Schönenberger C, Franse JJM, Menovsky AA (1987) Hall-effect and resistivity study of the heavy-fermion system URu_2Si_2. *Phys Rev B* 35:5375–5378.
26. Fontes MB, et al. (1999) Electron-magnon interaction in RNiBC (R=Er, Ho, Dy, Tb, and Gd) series of compounds based on magnetoresistance measurements. *Phys Rev B* 60:6781–6789.
27. Wolowiec CT (2016) The combined effect of pressure and Fe substitution on the ordered phases in the heavy fermion compound URu_2Si_2. *Phys Rev B* 94:085145.
28. Barron THK, White GK (1999) *Heat Capacity and Thermal Expansion at Low Temperatures* (Kluwer Academic/Plenum, New York).
29. Jeffries JR, Moore KT, Butch NP, Maple MB (2010) Degree of 5f electron localization in URu_2Si_2: Electron energy-loss spectroscopy and spin-orbit sum rule analysis. *Phys Rev B* 82:033103.
30. Wiebe CR, et al. (2007) Gapped itinerant spin excitations account for missing entropy in the hidden-order state of URu_2Si_2. *Nat Phys* 3:96–99.
31. Boariu FL, et al. (2013) Momentum-resolved evolution of the Kondo lattice into hidden order in URu_2Si_2. *Phys Rev Lett* 110:156404.
32. Meng JQ, et al. (2013) Imaging the three-dimensional Fermi-surface pairing near the hidden-order transition in URu_2Si_2 using angle-resolved photoemission spectroscopy. *Phys Rev Lett* 111:127002.
33. Oppeneer PM, et al. (2011) Spin and orbital hybridization at specifically nested Fermi surfaces in URu_2Si_2. *Phys Rev B* 84:241102(R).
34. Riseborough PS, Coqblin B, Magalhaes SG (2012) Phase transition arising from the underscreened Anderson lattice model: A candidate concept for explaining hidden order in URu_2Si_2. *Phys Rev B* 85:165116.